Chemical control of hole-doped superconductivity and magnetism in $Gd_{2-x}Ce_xRuSr_2Cu_2O_{10-\delta}$

A. C. Mclaughlin and J. P. Attfield*
Department of Chemistry, University of Cambridge, Lensfield Road, Cambridge CB2 1EW, United Kingdom and Interdisciplinary Research Centre in Superconductivity, Department of Physics, University of Cambridge, Madingley Road, Cambridge CB3 0HE, United Kingdom

U. Asaf and I. Felner
Racah Institute of Physics, The Hebrew University, Jerusalem, 91904, Israel
(Received 17 January 2003; published 10 July 2003)

Three $Gd_{2-x}Ce_xRuSr_2Cu_2O_{10-\delta}$ samples ($x=0.5$, as prepared and after high pressure oxygenation and $x=0.7$) have been investigated by synchrotron powder x-ray diffraction and magnetization measurements. Precise coordinates and site occupancies for the oxygen atoms have been refined from the x-ray experiments. Estimates of the hole doping of the copper oxide planes based on the bond lengths, via the bond valence sum method, are found to be inaccurate. However, doping estimates based on the refined oxygen contents are in good agreement with the variation of superconductivity, and show that chemical doping, rather Cu/Ru band overlap, is the doping mechanism. The magnetic ordering temperatures of the Ru moments are not a simple function of the doping concentration, but depend upon both the Gd/Ce ratio and the oxygen content.

DOI: 10.1103/PhysRevB.68.014503 PACS number(s): 74.72.Jt, 74.62.Dh, 74.62.Bf

INTRODUCTION

The unusual coexistence of weak ferromagnetism and superconductivity in the 2122 and 1212 ruthenocuprate[1–27] systems $R_{2-x}Ce_xRuSr_2Cu_2O_{10-\delta}$[2,3] ($R$=Eu and Gd) and $RuSr_2GdCu_2O_8$ (Ref. 4) has been studied extensively. The superconductivity originates in the CuO_2 planes and the weak ferromagnetism is associated with the ruthenate layers. μSR experiments have demonstrated that the materials are microscopically uniform with no evidence of spatial phase separation of superconducting and magnetic regions.[3–5] The Ru-2122 materials display a magnetic transition at $T_M = 125-215$ K and bulk superconductivity below $T_c = 32-50$ K depending on sample preparation and composition. Recent x-ray absorption near edge spectroscopy (XANES) and high-temperature susceptibility studies on $R_{2-x}Ce_xRuSr_2Cu_2O_{10}$ and $RuSr_2GdCu_2O_8$ have indicated that the average Ru valence state is 4.6 (Ref. 20) for $RuSr_2RCu_2O_8$ and between 5.0 and 4.95 (Refs. 24, 25) for $R_{2-x}Ce_xRuSr_2Cu_2O_{10}$. A mixed Ru valence has not been reported in other ruthenate compounds thus making the weak ferromagnetic superconductors $R_{2-x}Ce_xRuSr_2Cu_2O_{10}$ and $RuSr_2GdCu_2O_8$ intriguing materials to study and compare.

G-type antiferromagnetic order within the RuO_2 planes has been observed in neutron scattering experiments on $RuSr_2GdCu_2O_8$.[12] An upper limit of $0.1\mu_B$ was obtained for the ferromagnetic component, which appears to contradict results from SQUID magnetometry and electronic paramagnetic resonance experiments.[19] Variable field neutron diffraction studies of this material showed that the Ru spins cant into a ferromagnetic arrangement upon the application of a magnetic field and at 7 T the Ru spins are fully ferromagnetic. It is thought that the weak ferromagnetism arises via a canting of the Ru spins in $RuSr_2GdCu_2O_8$. This occurs due to the antisymmetric Dzyaloshinsky-Moriya interaction between neighboring Ru moments,[28,29] which is nonzero due to the tilts and rotations of the RuO_6 octahedra observed in synchrotron x-ray and neutron diffraction studies.[9–11] A recent neutron powder diffraction study has shown that rotations and tilts of the RuO_6 octahedra also occur in $Gd_{1.3}Ce_{0.7}RuSr_2Cu_2O_{10}$.[25] Furthermore a SQUID magnetometry study on $Eu_{2-x}Ce_xRuSr_2Cu_2O_{10-\delta}$[26] has shown that T_M increases with both Ce and oxygen concentration. T_M increases from 125 to 165 K as x increases from 0.5 to 1.0 in the $Eu_{2-x}Ce_xRuSr_2Cu_2O_{10-\delta}$ solid solutions and from 165 to 215 K as δ increases in the $EuCeRuSr_2Cu_2O_{10-\delta}$ solid solutions. It has been speculated that as the cerium concentration decreases there is a concomitant decrease in oxygen concentration δ.[25] This is in contrast to $RuSr_2GdCu_2O_8$, where the oxygen content remains constant upon doping with Nb or Sn.[30,31] Superconductivity only occurs for $x=0.4-0.8$ with optimal doping at $x=0.6$ in the 2122 system.[26] However the shift in T_c from the underdoped material to the optimal doped material is only 5 K which is much smaller than observed in the other high-temperature superconducting cuprates such as $La_{2-x}Sr_xCuO_4$. In order to observe any correlation between the changes in physical and magnetic properties with the crystal structure upon cerium and oxygen doping, synchrotron x-ray diffraction studies have been carried out for three $Gd_{2-x}Ce_xRuSr_2Cu_2O_{10-\delta}$ samples.

EXPERIMENTAL

Ceramic $Gd_{2-x}Ce_xRuSr_2CuO_{10-\delta}$ samples ($x=0.5$ and 0.7) were prepared by the solid state reaction of the stoichiometric oxides Gd_2O_3, CeO_2, $SrCO_3$, RuO_2, and CuO. These were ground, die-pressed into pellets and preheated for 24 h at 1000 °C. The samples were reground, repelleted and sintered for 36 h in air at 1064 °C and then furnace cooled to ambient temperature. Part of the ''as prepared'' (asp) $Gd_{1.5}Ce_{0.5}RuSr_2CuO_{10-\delta}$ sample was annealed for 24 h

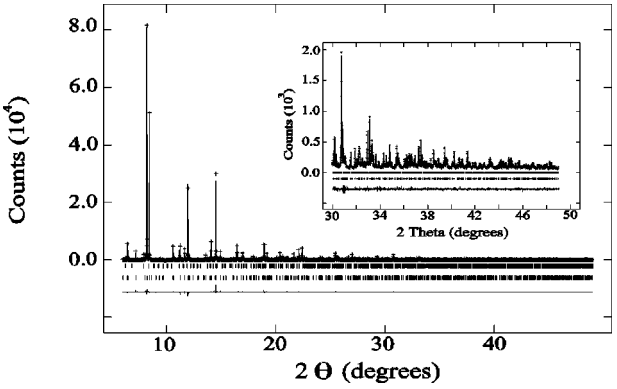

FIG. 1. Rietveld fit to the synchrotron x-ray diffraction pattern of $Gd_{1.3}Ce_{0.7}RuSr_2Cu_2O_{10}$. Lower and upper reflection marks correspond to $Gd_{1.3}Ce_{0.7}RuSr_2Cu_2O_{10}$ and the minority phase Sr_2GdRuO_6, respectively.

at 840 °C under high oxygen pressure (60 atm) and then furnace cooled to form a more oxygenated sample (hpo).

Powder synchrotron x-ray diffraction patterns of the $Gd_{-x}Ce_xRuSr_2CuO_{10-\delta}$ solid solutions were recorded on ESRF beamline ID31 (Ref. 32) at 295 K. A wavelength of 0.40027 Å was used and the sample was contained in a 0.5 mm diameter borosilicate glass capillary mounted on the axis of the diffractometer about which it was spun at ~1 Hz to improve the powder averaging of the crystallites. Diffraction patterns were collected over the angular range 2–50° 2θ. The high-angle parts of the pattern were scanned several times to improve the statistical quality of the data in these regions. The counts from the nine detectors were then normalized, summed and rebinned to a constant step size of 0.001° for each scan.

Zero-field cooled (ZFC) and field-cooled (FC) dc magnetic measurements in the range of 5–200 K were performed in a (Quantum Design) superconducting quantum interference device (SQUID) magnetometer. The ac susceptibility was measured by a home-made probe with excitation frequency and amplitude of 733 Hz and 160 mOe, respectively, inserted in the SQUID magnetometer.

RESULTS

The synchrotron x-ray diffraction patterns of $Gd_{1.5}Ce_{0.5}Sr_2RuCu_2O_{10-\delta}$ (asp) and (hpo), and $Gd_{1.3}Ce_{0.7}Sr_2RuCu_2O_{10-\delta}$ were all fitted by the Rietveld method using the GSAS program.[33] The backgrounds were fitted using linear interpolation and the peak shapes were modeled using a pseudo-Voigt function. The diffraction patterns showed that a small amount of Sr_2GdRuO_6 was present. This secondary phase was included in the refinements enabling excellent fits to be obtained (Fig. 1) for all samples using the $I4/mmm$ structural model for the 2212 phase. This model for $Gd_{2-x}Ce_xSr_2RuCu_2O_{10-\delta}$ is displayed in Fig. 2 and consists of RuO_2, SrO, and CuO_2 layers similar to $RuSr_2GdCu_2O_8$ but in this case the CuO_2 layers are separated by a $Gd_{2-x}Ce_xO_{2-\delta}$ block rather than a single rare earth layer. No evidence of superstructure or orthorhombic distortion was observed but disordered rotations and tilts of

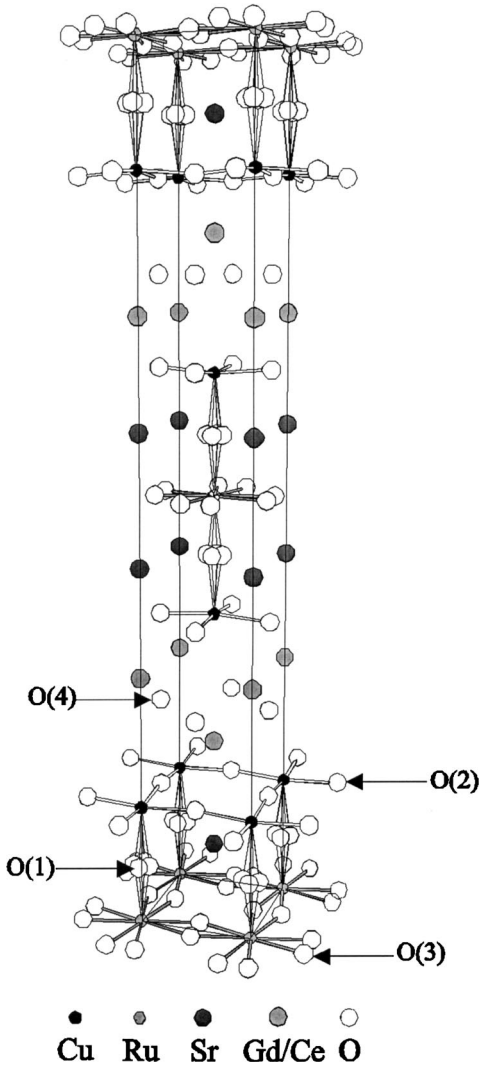

FIG. 2. The average crystal structure of $Gd_{2-x}Ce_xRuSr_2Cu_2O_{10-\delta}$ showing the tilts and rotations of the RuO_6 octahedra, with the oxygen sites labeled.

the RuO_6 octahedra were evidenced as previously seen in $RuSr_2GdCu_2O_8$ (Ref. 9) and $Pb_2RuSr_2Cu_2O_8Cl$.[32] These were modeled by splitting the oxygen sites of the RuO_6 octahedra as shown in Table I. All of the metal occupancies refined to within ±1% of full occupancy and there was no evidence of cation disorder. It has previously been reported that oxygen vacancies in $Gd_{2-x}Ce_xRuSr_2Cu_2O_{10-\delta}$ are located on the $O(4)$ site within the $Gd_{2-x}Ce_xO_{2-\delta}$ block.[27] To decorrelate the $O(4)$ occupancy from thermal motion, the occupancy was refined while also refining a single isotropic thermal parameter for all four oxygen sites. The refined $O(4)$ occupancies were 0.87(1) and 0.95(1) for (asp) and (hpo) $Gd_{1.5}Ce_{0.5}Sr_2RuCu_2O_{10-\delta}$, respectively. The $O(4)$ site was found to be fully occupied in $Gd_{1.3}Ce_{0.7}Sr_2RuCu_2O_{10-\delta}$. The increase in the c parameter (Table II) on going from (asp) to (hpo) $Gd_{1.5}Ce_{0.5}Sr_2RuCu_2O_{10-\delta}$ is in accordance with the incorporation of extra oxygen. The reduction in the a cell parameter

TABLE I. Refined atomic parameters for $RuSr_2(Gd_{2-x}Ce_x)Cu_2O_{10-d}$ solid solutions from room-temperature synchrotron x-ray diffraction data. Atom positions are Ru 2(*a*) (0, 0, 0), Sr 4(*e*) ($\frac{1}{2}$, $\frac{1}{2}$, *z*), Gd/Ce 4(*e*) ($\frac{1}{2}$, $\frac{1}{2}$, *z*), Cu 4(*e*) (0, 0, *z*), O(1) 16(*n*) (*x*, 0, *z*), O(2) 8(*g*) (0, $\frac{1}{2}$, *z*), O(3) 8(*j*) (*x*, $\frac{1}{2}$, 0), O(4) 4(*d*) (0, $\frac{1}{2}$, $\frac{1}{2}$).

			Sample (*x*)		
Atom	Occupancy		0.5 (asp)	0.5 (hpo)	0.7
Ru	1.00	U_{iso} (Å^2)	0.0034(2)	0.0048(1)	0.0053(1)
Sr	1.00	*z*	0.078 32(3)	0.078 54(3)	0.078 41(2)
		U_{iso} (Å^2)	0.0084(2)	0.0081(1)	0.0081(1)
Gd/Ce	1.00	*z*	0.204 70(2)	0.204 88(2)	0.205 14(2)
		U_{iso} (Å^2)	0.0083(1)	0.0054(1)	0.0038(1)
Cu	1.00	*z*	0.143 98(4)	0.143 73(4)	0.143 67(3)
		U_{iso} (Å^2)	0.0060(2)	0.0018(2)	0.0024(1)
O(1)	0.25	*x*	0.021(6)	0.033(3)	0.046(2)
		z	0.0692(2)	0.0687(2)	0.0685(2)
		U_{iso} (Å^2)	0.0187(7)	0.0179(6)	0.0125(4)
O(2)	1.00	*z*	0.1498(2)	0.1481(2)	0.1483(1)
		U_{iso} (Å^2)	0.0187(7)	0.0179(6)	0.0125(4)
O(3)	0.50	*x*	0.125(2)	0.134(2)	0.130(2)
		U_{iso} (Å^2)	0.0187(7)	0.0179(6)	0.0125(4)
O(4)	*n*	U_{iso} (Å^2)	0.0187(7)	0.0179(6)	0.0125(4)
		n	0.87(1)	0.95(1)	1.0

TABLE II. Refined cell data, agreement factors, and selected bond lengths (Å) and angles (deg.) for the $RuSr_2Gd_{2-x}Ce_xCu_2O_{10}$ samples. The ranges of O(1)-Cu-O(2) angles result from the disordered tilts of the RuO_6 octahedra.

	Sample (*x*)		
	0.5 (asp)	0.5 (hpo)	0.7
a (Å)	3.83815(1)	3.83772(1)	3.83809(1)
c (Å)	28.58961(7)	28.59334(1)	28.58528(5)
V (Å^3)	421.165(2)	421.126(7)	421.088(1)
χ^2	4.17	3.83	4.37
R_{WP} (%)	12.5	11.9	12.7
R_P (%)	9.3	8.4	8.3
Gd/Ce-O(2)×4	2.479(3)	2.514(3)	2.514(2)
Gd/Ce-O(4)×4	2.3154(3)	2.3123(2)	2.3081(2)
Cu-O(1)×1	2.139(6)	2.148(5)	2.157(5)
Cu-O(2)×4	1.9263(4)	1.9229(3)	1.9236(3)
Sr-O(1)×2	2.67(2)	2.639(9)	2.608(6)
Sr-O(1)×2	2.78(2)	2.820(9)	2.856(6)
Sr-O(2)×4	2.804(3)	2.764(3)	2.770(3)
Sr-O(3)×2	2.662(4)	2.648(4)	2.654(3)
Sr-O(3)×2	3.281(6)	3.312(5)	3.296(4)
Ru-O(1)×2	1.981(6)	1.970(5)	1.965(4)
Ru-O(3)×4	1.978(2)	1.987(2)	1.982(1)
O(1)-Cu-O(2)	95.0–97.1(5)	90.3–97.1(4)	89.2–98.6(1)
Cu-O(1)-Ru	175.6(9)	172.8(5)	170.2(5)
Cu-O(2)-Cu	170.1(3)	172.6(3)	172.1(2)
Ru-O(3)-Ru	152.0(5)	149.9(3)	150.9(3)

on going from (asp) to (hpo) $Gd_{1.5}Ce_{0.5}Sr_2RuCu_2O_{10-\delta}$ and $Gd_{1.7}Ce_{0.3}Sr_2RuCu_2O_{10-\delta}$ increases the rotations and tilts of the RuO_6 octahedra, respectively quantified by the Ru-O(3)-Ru and Cu-O(1)-Ru angles in Table II.

Figure 3 shows the temperature dependence of the normalized ac susceptibility curves (at $H_{dc}=0$) for the $Gd_{2-x}Ce_xRuSr_2Cu_2O_{10-\delta}$ samples. $Gd_{1.5}Ce_{0.5}Sr_2RuCu_2O_{10-\delta}$ (asp) is not superconducting but superconductivity is observed for $Gd_{1.5}Ce_{0.5}Sr_2RuCu_2O_{10-\delta}$ (hpo) and $Gd_{1.3}Ce_{0.7}Sr_2RuCu_2O_{10-\delta}$ with onset T_C's of 28 and 30 K, respectively. Similar results were obtained from dc magnetization studies, where T_C is defined as the local maximum maximum in the ZFC data (Figs. 4 and 5). It is possible that the drop at 16 K for (asp) $Gd_{1.5}Ce_{0.5}Sr_2RuCu_2O_{10-\delta}$ arises from a small fraction of a superconducting phase not detected in the dc magnetization studies. The peaks in the ac

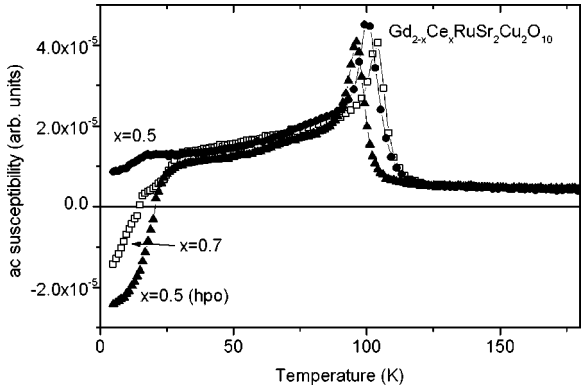

FIG. 3. Normalized ac susceptibility, measured at $H_{dc}=0$ of the $Gd_{2-x}Ce_xRuSr_2Cu_2O_{10-\delta}$ samples.

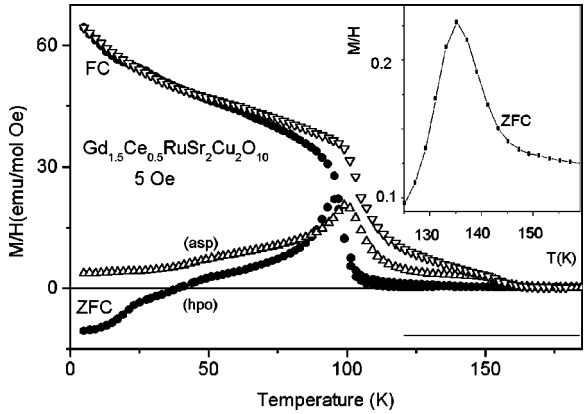

FIG. 4. ZFC and FC M/H curves for $Gd_{2-x}Ce_xRuSr_2Cu_2O_{10-\delta}$ (asp) and (hpo) samples. The expanded inset shows the antiferromagnetic ordering peak in the ZFC branch of the hpo sample.

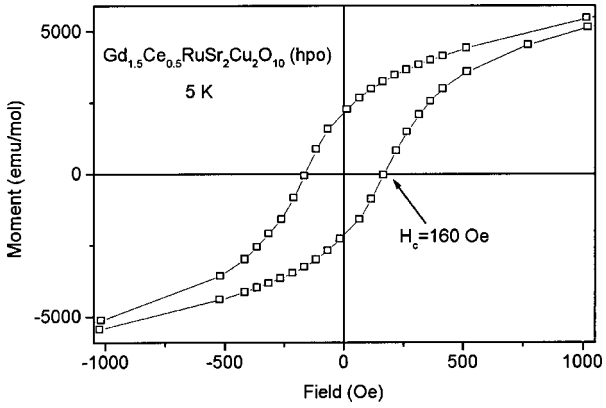

FIG. 6. Magnetic hysteresis loop for (hpo) $Gd_{1.5}Ce_{0.5}RuSr_2Cu_2O_{10}$ with the coercive field shown.

curves mark the irreversibility temperature, T_{irr} discussed below.

Evidence of the Meissner effect is observed in the ZFC magnetization measurements of $Gd_{1-x}Ce_xRuSr_2Cu_2O_{10}$ [$x=0.5$ (hpo), $x=0.7$] [Figs. 4 and 5]. The FC branches appear ferromagnetic, but antiferromagnetic behavior is observed in the ZFC measurements. The ZFC and FC curves merge at $T_{irr}=104$, 100, and 96 K for $x=0.7$, $x=0.5$ (asp) and $x=0.5$ (hpo), respectively. Hence T_{irr} decreases with oxygen doping but increases with Ce doping, consistent with previous results.[3] The M/H curves do not lend themselves to an easy determination of T_M(Ru), which was obtained for all samples directly from the temperature dependence of the saturation moment (M_{sat}), as below.

Variable field magnetization studies were performed at various temperatures for all samples. The variation of magnetization with field can be described as $M(H)=M_{sat}+\chi_0 H$, where M_{sat} corresponds to the weak ferromagnetic contribution of the Ru sublattice, and $\chi_0 H$ is the linear paramagnetic contribution of Gd and Cu. The saturation moment for $Gd_{1.3}Ce_{0.7}Sr_2RuCu_2O_{10-\delta}$ at 5 K is $M_{sat}\sim 1\mu_B$. $M(H)$ curves were measured at various temperatures and a reduction in M_{sat} is observed with decreasing temperature until T_M(Ru), where $M_{sat}=0$; T_M(Ru)$=165$, 151, and 142 K for $Gd_{1.3}Ce_{0.7}Sr_2RuCu_2O_{10}$, $Gd_{1.5}Ce_{0.5}Sr_2RuCu_2O_{10-\delta}$ (asp) and $Gd_{1.5}Ce_{0.5}Sr_2RuCu_2O_{10-\delta}$ (hpo) respectively. Hence T_M also increases with Ce doping but decreases with oxygen doping consistent with previous results.[26,34]

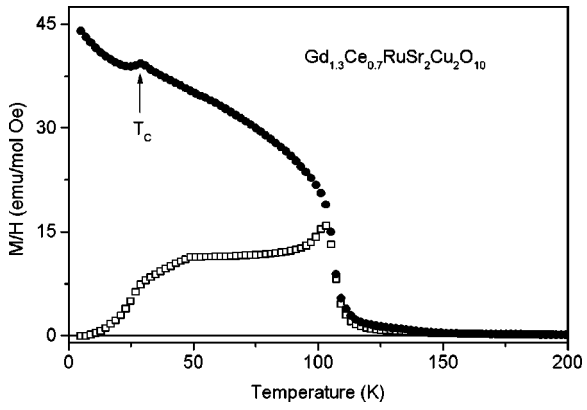

FIG. 5. ZFC and FC susceptibility curves for $Gd_{1.3}Ce_{0.7}RuSr_2Cu_2O_{10}$ measured at $H=3$ Oe. T_C is shown at the deflection in the FC branch.

At low applied fields, the $M(H)$ curve exhibits a typical ferromagneticlike hysteresis loop (Fig. 6) similar to that previously reported.[3] The remnant moment ($M_{rem}=0.41\mu_B$/Ru) and the coercive field ($H_C=-160$ Oe at 5 K) are the same for all samples.

DISCUSSION

Knowledge of the cation and oxygen content of cuprates is important for making a chemical estimate of the hole concentration via the formal Cu oxidation state. Diffraction analysis has the advantage of giving an accurate composition for well-crystallized materials even when secondary phases are present, as here. The high peak to background ratio of the present synchrotron x-ray data permits refinement of the occupancy of the $O(4)$ site within the double R layers of these 2212 structures. The Rietveld refinements show that the occupancy of $O(4)$ increases from 0.87 to 0.95 to 1.00 for $Gd_{1.5}Ce_{0.5}Sr_2RuCu_2O_{10-\delta}$ (asp), $Gd_{1.5}Ce_{0.5}Sr_2RuCu_2O_{10-\delta}$ (hpo), and $Gd_{1.3}Ce_{0.7}Sr_2RuCu_2O_{10}$, respectively. Substitution of Ce^{4+} for Gd^{3+} at constant oxygen content would lead to a reduction in the hole-doping of the copper or ruthenium layers. However, in the 2212 structure, the two ($Gd_{1-x/2}Ce_{x/2}$) layers sandwich the defective $O(4)$ layer so the increase in the cation layer charge with x can be charge compensated by an increase of the $O(4)$ content. Increasing from $x=0.5$ to 0.7 requires only an increase of 0.05 in the $O(4)$ occupancy for charge compensation. Comparison of $Gd_{1.5}Ce_{0.5}Sr_2RuCu_2O_{10-\delta}$ (asp) and $Gd_{1.3}Ce_{0.7}Sr_2RuCu_2O_{10}$, which were prepared under identical conditions, shows an increase of 0.13(1) in the $O(4)$ occupancy, so that the increase in Ce^{4+} concentration (x) is actually *overcompensated* by the increase in oxygen content. This results in an increased hole doping, contrary to what

would have been expected from the Ce substitution alone. The hole doping is corroborated by comparing the formal charges derived from the overall chemical composition to the superconducting properties. The formal positive charge for (2Cu+Ru) is calculated as 8.98, 9.30, and 9.30 for the compositions $Gd_{1.5}Ce_{0.5}Sr_2RuCu_2O_{9.74}$ (asp), $Gd_{1.5}Ce_{0.5}Sr_2RuCu_2O_{9.90}$ (hpo), and $Gd_{1.3}Ce_{0.7}Sr_2RuCu_2O_{10}$, respectively.

The ac susceptibility measurements show the (asp) sample to be nonsuperconducting but the other two samples have very similar T_c's of 28 and 30 K. This suggests a formal charge distribution within error of $2Cu^{2+}+Ru^{5+}$ in the (asp) sample, with no doping of the copper oxide planes, whereas the latter two samples are both $2Cu^{2+p+}+Ru^{5+}$ with $p=0.15$. This corresponds to near-optimum doping of the copper oxide planes.

We have also attempted to estimate the charge distribution between Cu and Ru using bond valence sums (BVS) which are based on the refined Cu-O bond lengths. The copper valence was calculated using with standard values of $r_0=1.679$ and 1.73 Å for Cu^{2+} and Cu^{3+} respectively,[35] yielding values of 2.52, 2.54, and 2.52 for $Gd_{1.5}Ce_{0.5}Sr_2RuCu_2O_{10-\delta}$ (asp), $Gd_{1.5}Ce_{0.5}Sr_2RuCu_2O_{10-\delta}$ (hpo), and $Gd_{1.3}Ce_{0.7}Sr_2RuCu_2O_{10}$. It is well documented that BVS overestimates the hole doping in the ruthenocuprate materials;[10] for example, $RuSr_2GdCu_2O_8$ has been found to have $p=0.08$ based on superconducting and normal state transport properties, but BVS calculations estimate the Cu valence as 2.4. This results from the presence of an apical Cu-O bond that is anomalously short in comparison to the other superconducting cuprate structures. Furthermore, the three BVS estimates for the present 2212 materials are not significantly different, so they do not account for the difference between the nonsuperconducting (asp) and the superconducting (hpo) and $x=0.7$ samples. This is also in keeping with a previous study of doped $Ru_{1-x}M_xSr_2GdCu_2O_8$ samples ($M=$Nb,Sn),[31] in which physical measurements showed an increase in hole doping of the CuO_2 planes with Sn substitution and a decrease with Nb substitution. However, there was no corresponding trend of the Cu BVS with doping.

Examining the individual geometric parameters in Table II, it is evident that the change from nonsuperconducting (asp) to superconducting (hpo) and $x=0.7$ samples correlates with an increase in the Cu-O(2)-Cu angles (from 170° to 172°). The flattening of the CuO_2 planes is known to correlate with increasing superconductivity in cuprates, and is clearly a more sensitive indicator than the Cu BVS here.

We conclude that BVS calculations of Cu valence are insensitive to the carrier concentrations in ruthenocuprate materials and the best chemical estimate is obtained from determination of the composition. The substitution of Ce for Gd in the structure of $Gd_{2-x}Ce_xSr_2RuCu_2O_{10-\delta}$ is overcompensated by an increase in the oxygen content leading to an increase in the hole doping. Hence, in order to obtain the correct electronic phase diagram of $Gd_{2-x}Ce_xSr_2RuCu_2O_{10-\delta}$ it is imperative that the oxygen stoichiometry is measured. X-ray absorption spectroscopy could also be used to investigate the hole distribution in phase pure materials.

The qualitative magnetic behavior of the Ru-2122 system[26] is as follows. Starting from high to low temperatures, the magnetic behavior is divided into four regions. (i) Above T_M(Ru) the system is paramagnetic. (ii) At T_M which is deduced directly from the temperature dependence of $M_{\rm sat}$, the Ru sublattice becomes antiferromagnetically ordered. The up rise at elevated temperature of the ZFC branch (Fig. 4 inset) indicates precisely this antiferromagnetic behavior. (iii) At $T_{\rm irr}$ a weak ferromagnetism is induced, which originates from canting of the Ru moments. $T_{\rm irr}$ is defined as the merging point of the low field ZFC and FC branches, or alternatively, as the peak in the ac curves. Canting of the Ru moments may arise from a Dzyaloshinsky-Moriya interaction between neighboring moments which is nonzero due to symmetry-breaking tilts and rotations of the RuO_6 octahedra. (iv) At lower temperatures superconductivity is induced and T_C depends strongly on Ce and on oxygen concentrations as shown in Fig. 3. Below T_C, both superconductivity and weak-ferromagnetic states coexist and the two states are practically decoupled.

We have shown that both $T_{\rm irr}$ and T_M are affected by oxygen and Ce doping in the $Gd_{2-x}Ce_xRuSr_2Cu_2O_{10-\delta}$ system; both T_M and $T_{\rm irr}$ increase with Ce doping but decrease with oxygen doping. There is no drastic change in the crystal structure with either Ce or oxygen doping. Both $Gd_{1.5}Ce_{0.5}RuSr_2Cu_2O_{10-\delta}$ (hpo) and $Gd_{1.3}Ce_{0.7}RuSr_2Cu_2O_{10}$ have the same charge states for Cu and Ru and the local environments around Ru are the same, suggesting a different influence for the different magnetic transition temperatures such as the Gd/Ce ratio. Recent XANES and high-temperature susceptibility studies on $R_{2-x}Ce_xRuSr_2Cu_2O_{10}$ and $RuSr_2GdCu_2O_8$ have indicated that the average Ru valence state is 4.6 (Ref. 20) for $RuSr_2RCu_2O_8$ and between 5.0 and 4.95 (Refs. 24, 25) for $R_{2-x}Ce_xRuSr_2Cu_2O_{10}$ suggesting the Ru valence is not significantly reduced below 5.0 in $R_{2-x}Ce_xRuSr_2Cu_2O_{10}$ materials, in keeping with the present analysis. The main structural difference between $Gd_{1.5}Ce_{0.5}RuSr_2Cu_2O_{10-\delta}$ (hpo) and $Gd_{1.3}Ce_{0.7}RuSr_2Cu_2O_{10}$ is the c lattice parameter; c increases from 28.590 to 28.593 Å as oxygen is incorporated into $Gd_{1.5}Ce_{0.5}RuSr_2Cu_2O_{10-\delta}$, whereas c decreases from 28.590 to 28.585 Å as x increases to 0.7. As the concentration of Ce increases, there is a resultant increase of oxygen into the structure but the decrease of c due to the addition of the smaller Ce cation outweighs the structural effects of oxygen insertion. A recent report[36] showed how the magnetic behavior of $Gd_{2-x}Ce_{0x}RuSr_2Cu_2O_{10-\delta}$ is different from that of $RuSr_2GdCu_2O_8$; magnetic logarithmic relaxation, inverted hysteresis loops and metastable magnetic states were observed. It was concluded that a long range dipole-dipole interaction between RuO_2 layers exists which is antiferromagnetic in zero field. Upon application of a small field ($<$100 Oe) the interlayer magnetic coupling becomes ferromagnetic due to a spin flop interaction. It appears that small changes in the interlayer axis affect this interaction so that the dipole-dipole interaction becomes weaker with increasing c and both T_M and $T_{\rm irr}$ decrease.

CONCLUSIONS

From this study, in conjunction with previous works on ruthenocuprate materials, commonalities and differences between the three families (1212, 2122, and $Pb_2RuSr_2Cu_2O_8Cl$) are evident. All of these structures have commensurate CuO_2 and RuO_2 planes so that the mismatch between the Cu-O and the (longer) Ru-O bonds always results in rotations and tilts of the RuO_6 octahedra. The resulting strains within these structures may account for the poor correlation of physical properties with BVS's, although these are known to correlate well in other cuprates. The local symmetry-breaking distortions can lead to nonzero antisymmetric exchange responsible for the weak ferromagnetism observed in addition to the underlying Ru-layer antiferromagnetism in all three types of ruthenocuprate. The other Ru-layer magnetic phenomena depend on the interlayer couplings which vary due to the different connectivities, distances, and intermediate diamagnetic or paramagnetic ions. In the present 2122 samples, T_M and $T_{\rm irr}$ decrease with oxygen doping but increase with Ce doping due to the interplay of the latter factors.

The principal requirement for superconductivity in all cuprates is a doping of the CuO_2 planes, usually with holes in the range $p \approx 0.05-0.25$. The mechanism for doping in the 1212 material $RuSr_2GdCu_2O_8$ was previously established as being Cu/Ru band overlap, with estimated valences of Ru $+4.84$ and Cu $+2.08$. This is rather rare in cuprates, the only well-established examples involve homometallic band overlap (of Cu chains and planes) in $RBa_2Cu_3O_7$ and related materials. The Ru-1212 are arguably the only examples of cuprate superconductors doped by heterometallic band overlap (of Ru and Cu planes). This study demonstrates that the Ru-2122 superconductors are doped not by band overlap, but by variations in the cation and oxygen content as is typical for most cuprates (doped-La_2CuO_4; Bi, Tl, and Hg cuprates, etc.). Thus, an increase of the $O(4)$ site occupancy between the R bilayers is achieved by annealing $Gd_{1.5}Ce_{0.5}RuSr_2Cu_2O_{10-\delta}$ under high pressure oxygen or by increasing the Ce content to $x=0.7$. This results in the same Cu doping of ~ 0.15 holes/Cu in both (hpo) $Gd_{1.5}Ce_{0.5}RuSr_2Cu_2O_{10-\delta}$ and $Gd_{1.3}Ce_{0.7}RuSr_2Cu_2O_{10}$, which is corroborated by their T_c's of 28 and 30 K, respectively, whereas $Gd_{1.5}Ce_{0.5}RuSr_2Cu_2O_{10-\delta}$ (asp) is undoped and nonsuperconducting. All of these 2122 materials contain fully oxidized Ru^{5+}.

ACKNOWLEDGMENTS

This research was supported by the Israel Academy of Science and Technology (2000), the Klachky Foundation for Superconductivity, and by EPSRC, UK.

*Email address: jpa14@cam.ac.uk

[1] L. Bauernfeind, W. Widder, and H. F. Braun, Physica C **254**, 151 (1995).
[2] L. Bauernfiend, W. Widder, and H. F. Braun, J. Low Temp. Phys. **105**, 1605 (1996).
[3] I. Felner, U. Asaf, Y. Lavi, and O. Milio, Phys. Rev. B **55**, 3374 (1997).
[4] J. L. Tallon, C. Bernhard, M. Bowden, P. Gilberd, T. Stoto, and D. Pringle, IEEE Trans. Appl. Supercond. **9**, 1696 (1999).
[5] C. Bernhard, J. L. Tallon, C. Niedermayer, T. Blasius, A. Golnik, E. Brucher, R. K. Kremer, D. R. Noakes, C. E. Stronach, and E. J. Ansaldo, Phys. Rev. B **59**, 14 099 (1999).
[6] K. B. Tang, Y. T. Qian, L. Yang, Y. D. Zhao, and Y. H. Zhang, Physica C **282-287**, 947 (1997).
[7] I. Felner, U. Asaf, S. Reich, and Y. Tsabba, Physica C **163**, 311 (1999).
[8] J. L. Tallon, J. W. Loram, G. V. M. Williams, and C. Bernhard, Phys. Rev. B **61**, 6471 (2000).
[9] A. C. Mclaughlin, W. Zhou, J. P. Attfield, A. N. Fitch, and J. L. Tallon, Phys. Rev. B **60**, 7512 (1999).
[10] A. C. Mclaughlin, J. P. Attfield, and J. L. Tallon, Int. J. Inorg. Mater. **2**, 95 (2000).
[11] O. Chmaissam, J. D. Jorgensen, H. Shaked, P. Dollar, and J. L. Tallon, Phys. Rev. B **61**, 6401 (2000).
[12] J. W. Lynn, B. Keimer, C. Ulrich, C. Bernhard, and J. L. Tallon, Phys. Rev. B **61**, 14 964 (2000).
[13] X. H. Chen, Z. Sun, K. Q. Wang, S. Y. Li, Y. M. Xiong, M. Yu, and L. Z. Cao, Phys. Rev. B **63**, 064506 (2001).
[14] K. Nakamura, K. T. Park, A. J. Freeman, and J. D. Jorgensen, Phys. Rev. B **63**, 024507 (2001).
[15] Y. Furukawa, S. Takada, A. Yamanaka, and K. Kumagai K, Physica C **341**, 453 (2000).
[16] C. Bernhard, J. L. Tallon, E. Brucher, and R. K. Kremer, Phys. Rev. B **61**, 14 960 (2000).
[17] A. Fainstein, P. Etchegoin, H. J. Trodahl, and J. L. Tallon, Phys. Rev. B **61**, 15 468 (2000).
[18] A. Butera, A. Fainstein, E. Winkler, and J. L. Tallon, Phys. Rev. B **63**, 054442 (2001).
[19] A. Fainstein, E. Winkler, A. Butera, and J. L. Tallon, Phys. Rev. B **60**, 12 597 (1999).
[20] J. D. Jorgensen, O. Chmaissem, H. Shaked, S. Short, P. W. Klamut, B. Dabrowski, and J. L. Tallon, Phys. Rev. B **63**, 054440 (2001).
[21] R. S. Liu, L. Y. Jang, H. H. Hung, and J. L. Tallon, Phys. Rev. B **63**, 212507 (2001).
[22] A. V. Boris, P. Mandal, C. Bernhard, N. N. Kovaleva, K. Pucher, J. Hemberger, and A. Loidl, Phys. Rev. B **63**, 184505 (2001).
[23] G. V. M. Williams and S. Krämer, Phys. Rev. B **62**, 4132 (2000).
[24] I. Felner, U. Asaf, C. Godart, and E. Alleno, Physica B **259–261**, 703 (1999).
[25] G. V. M. Williams, L.-Y. Jang, and R. S. Liu, Phys. Rev. B **65**, 064508 (2002).
[26] I. Felner, U. Asaf, and E. Galstyan, Phys. Rev. B **66**, 024503 (2002).
[27] C. S. Knee, B. D. Rainford, and M. T. Weller, J. Mater. Chem. **10**, 2445 (2000).
[28] I. Dzyaloshinksy, Sov. Phys. JETP **5**, 1259 (1957).
[29] T. Moriya, Phys. Rev. **120**, 91 (1960).
[30] A. C. Mclaughlin, V. Janowitz, J. A. McAllister, and J. P. Attfield, Chem. Commun. **2000**, 1331.
[31] A. C. Mclaughlin, V. Janowitz, J. A. McAllister, and J. P. Attfield, J. Mater. Chem. **11**, 173 (2000).
[32] A. C. Mclaughlin, J. A. McAllister, L. D. Stout, and J. P. Attfield,

Phys. Rev. B **65**, 172506 (2002).
[33] A. C. Larson and R. B. Von Dreele, General Structure Analysis System (GSAS) Report No. LAUR 86-748, Los Alamos National Laboratory, 1994 (unpublished).
[34] I. Felner, U. Asaf, F. Ritter, P. W. Klamut, and B. Dabrowski, Physica C **364-365**, 368 (2001).
[35] I. D. Brown, J. Solid State Chem. **82**, 122 (1989).
[36] I. Zivkovic, Y. Hirai, B. H. Frazer, M. Prester, D. Drobac, D. Ariosa, H. Berger, D. Pavuna, and G. Margaritondo, Phys. Rev. B **65**, 144420 (2002).